Journal of Statistical Physics, Vol. 73, Nos. 5/6, 1993

Review of New Experimental Techniques for Investigating Random Sequential Adsorption

J. J. Ramsden[1]

Received March 3, 1993; final July 29, 1993

Burgeoning interest in random sequential adsorption (RSA) processes has led to a surge of theoretical results, but experimental work is lagging behind, due to a dearth of suitable techniques. This article reviews integrated-optical techniques for investigating the kinetics of RSA and related processes. The basic idea is to measure the phase shifts of guided waves, due to the adsorption of particles at the surface of a planar waveguide. The technique is very well suited to investigating 2-dimensional RSA, and can yield high-quality kinetic adsorption data, precise enough for rigorously testing theoretical predictions. The current state of the art allow adsorbed mass to be measured quasicontinuously with a precision of at least 1 ng/cm^2.

KEY WORDS: Random sequential adsorption; deposition kinetics; integrated optics; planar waveguides; grating coupler.

1. INTRODUCTION

In a random sequential deposition or adsorption (RSA) process, particles are placed consecutively at random on a solid surface, such that they do not overlap. The basic model assumes that the surface is smooth and the particles are rigid and uniform; each particle arriving in the vicinity of the surface from the bulk in which they are suspended either adheres to the surface or, if a least part of its chosen site is already occupied, departs back into the bulk. The topic has excited the interest of theoreticians at least since 1957, when Rényi solved the simplest, one-dimensional problem ("random car parking").[1] Rényi himself intended the 1D case as a stepping stone to the 2- and 3-dimensional cases, but in dimensions higher

[1] Department of Biophysical Chemistry, Biozentrum, CH-4056 Basle, Switzerland, and Department of Chemical Engineering, ETH, CH-8092 Zürich, Switzerland.

0022-4715/93/1200-0853$07.00/0

than 1 the problem is much more difficult to solve, and no analytic solutions have been found. Yet for 2 dimensions in particular, the range of natural phenomena which can be described by RSA and its extensions (involving mixtures of different kinds of particles, anisotropic particles, postadsorption relaxation etc.) is very large.[2] There is rapidly growing interest in the field,[2] but until now the main results have been theoretical.

In contrast, the experimental situation is much less satisfactory, and few reliable results have been reported. The main reason seems to be the dearth of suitable experimental techniques. In order for useful data to be acquired which can be accurately compared with theory, it is necessary to have both good time and mass or particle number resolution. In many methods used to investigate adsorption phenomena, these two requirements are mutually exclusive: reliable, absolute mass determinations are slow to carry out, and so preclude kinetic measurements, whereas rapid measurement techniques either yield only the relative numbers of absorbed particles or are insufficiently precise for comparing with theoretical predictions.

One of the first quantitative adsorption experiments was that of Brillouin, undertaken at the instigation of Perrin, to determine Avogadro's number from the kinetics of deposition of gamboge particles on a glass slide.[3] Conditions had been found under which the probability that a particle colliding with the glass would adhere was very high, exceeding 0.95. The adsorbed particles were counted by observing the slide under an optical microscope. A later report[6] used a similar technique for the determination of the jamming limit for spherical latex particles in two dimensions. Although the technique has the advantage of arbitrarily high precision, in the sense that a single particle can be observed regardless of the total substrate area, and by taking a rapid sequence of photomicrographs could also be adapted to kinetic measurements, it is somewhat cumbersome, and only applicable to particles visible in the optical microscope, i.e., larger than a few hundred nanometers. Many natural RSA phenomena involve

[2] In addition to numerous natural phenomena, one should also include the vast field of technical applications, such as deposition of material onto the walls of reaction vessels, tubing, and filters in chemical plants; the deposition of blood proteins on artificial implants in medicine; and the deposition of material on teeth. Many technologies involve the deposition of particles at a surface, e.g., the coating of transducer plates with selective receptors in chemical sensor technology. It has furthermore recently been shown by numerical simulation that adsorption processes taking diffusion[3] and hydrodynamic interactions[4] into account are remarkably well approximated by the simple RSA model. When *both* are taken into account the agreement is excellent,[4] suggesting that the effective neglect of both in RSA fortuitiously cancels out their effects.

[3] The experiment is discussed by Smoluchowski.[5]

molecules too small to be investigated in this way. If the adsorption of small molecules can be detected, flexibility in the design of experiments is enormously increased.[4]

An elegant new technique for the investigation of adsorption at a planar surface has been provided by integrated optics, a rather new field of activity based on the fact that light can be confined in very thin films (i.e., of dimensions $\sim\lambda$, where λ = light wavelength) of transparent materials, the refractive index n_F of the thin film F being greater than the refractive index of the surroundings. These thin-film structures are called optical waveguides. A planar waveguide is used as the surface on which adsorption of particles takes place. The number of absorbed particles can be determined continuously *in situ* by measuring changes in the phase velocities of guided modes, changes which are engendered by the formation of an adlayer of adsorbed particles on the waveguide surface. The current mass resolution of the method is about 1 ng/cm^2.

In the remainder of this article, salient concepts of integrated optics will be reviewed with specific reference to RSA.

2. OVERVIEW OF INTEGRATED OPTICS

2.1. The Mode Equation

When a ray of light impinges with angle θ to the normal of a planar boundary between two dielectrics, let us say F and J, with refractive indices respectively n_F and n_J, according to the well-known Snell's law,[5] the refracted beam propagates away from the interface with an angle θ_J to the interface normal, given by

$$n_F \sin\theta = n_J \sin\theta_J \tag{1}$$

Assume $n_F > n_J$, and let θ increase from 0. When $\sin\theta = n_J/n_F$, $\sin\theta_J = 1$, and since it cannot exceed 1, further increase in θ results in *total internal reflection* at the interface. Let F be a thin dielectric film (the optical waveguide) bounded by media with lower refractive indices: a light ray can be trapped in F and propagate via total internal reflection alternately

[4] Furthermore, truly diffusive (uncorrelated) motion only sets in on a time scale $\sim 10^3\tau$,[7] where $\tau = a^2/\nu$ is the hydrodynamic time scale characterizing the particle (radius = a) velocity autocorrelation function (ν is the kinematic viscosity of the solvent). For an $a = 10\ \mu$m colloidal particle in water, $\tau \approx 0.1$ msec, whereas for a protein ($a = 10$ nm), $\tau \approx 10$ fsec. Therefore the usual assumption of uncorrelated motion is not valid for colloidal particles on subsecond time scales.

[5] This law was discovered some decades before Snell by T. Harriott.[8]

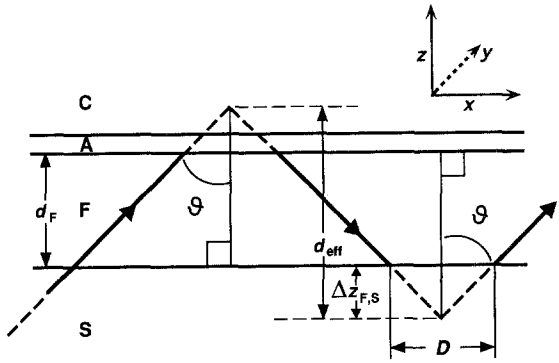

Fig. 1. Ray-optic representation of a guided wave propagating in the thin film F, showing the various quantities referred to in the text. The layers are conventionally denoted S (support), F (film), A (adlayer), and C (cover). The support is needed to give the thin film F adequate mechanical strength. D ($=2\Delta z_{F,J} \tan \theta$) is the lateral displacement of the reflected beam.

at each interface with an angle of incidence $\arcsin n_J/n_F < \theta < \pi/2$ (Fig. 1). This is the basis for integrated optics. The propagation constant β is defined as the wave component parallel to the waveguide, i.e., $\beta = kn_F \sin \theta$, where $k = 2\pi/\lambda$ is the free-space wave number. The effective refractive index or mode index N of the composite waveguide structure (comprising waveguiding film and surroundings) is given by

$$N = \beta/k = \beta c/\omega = n_F \sin \theta \tag{2}$$

where c is the vacuum velocity of light and ω its angular frequency; the phase velocity v parallel to the film is c/N. The wave component $k_{z,F}$ perpendicular to the waveguide is $kn_F \cos \theta$, which, using the above definition of N, can be written as

$$k_{z,F} = k(n_F^2 - N^2)^{1/2} = kn_F \cos \theta \tag{3}$$

The details of what actually occurs upon total internal reflection have prompted much inquiry. Newton supposed that the light went some way into the rarer medium J before returning to F.[9,10] This speculation turned out not to be so far from the truth: in 1947 Goos and (Lindberg)-Hänchen[11] established that upon total internal reflection, the beam incident on the reflecting interface undergoes a small lateral shift D before returning to the medium whence it came (Fig. 1); in effect, the light penetrates some way into the external medium J before being reflected at an imaginary plane situated at a distance $\Delta z_{F,J}$ from the F, J dielectric discontinuity. The magnitude of the penetration distance is[12,13]

$$\Delta z_{F,J} = 1/\{|k_{z,F}| [(N/n_F)^2 + (N/n_J)^2 - 1]^{\rho}\} \tag{4}$$

where ρ equals 0 and 1 for transverse electric (TE) and transverse magnetic (TM) waves, respectively.[6] For typical practical devices, $\Delta z_{F,J} \sim 100$ nm.

The starting point for deriving the field distribution in and around the waveguide is Maxwell's equations. The refractive index is assumed to vary in the z direction only; the problem is analogous to that of a quantum mechanical particle confined in a 1-dimensional box by walls of finite height and thickness. For TE waves, Maxwell's curl equations are[14]

$$\begin{aligned} \varepsilon_0 n(z)^2\, \partial E_y/\partial t &= \partial H_x/\partial z - \partial H_z/\partial x \\ \mu_0\, \partial H_x/\partial t &= \partial E_y/\partial z \\ -\mu_0\, \partial H_z/\partial t &= \partial E_y/\partial x \\ \partial H_x/\partial x + \partial H_z/\partial z &= 0 \end{aligned} \tag{5}$$

for an isotropic, linear, nonconducting, charge-free, and nonmagnetic material. By eliminating H_x and H_z from the first three equations, one obtains $[n^2(z)/c^2]\, \partial^2 E_y/\partial t^2 = \partial^2 E_y/\partial x^2 + \partial^2 E_y/\partial z^2$, representing plane waves travelling in the x direction. Hence we look for solutions of the form

$$\begin{aligned} E_y &= E_y(z) \exp[i(\omega t - \beta x)] \\ H_x &= H_x \exp[i(\omega t - \beta x)] \\ H_z &= H_z \exp[i(\omega t - \beta x)] \end{aligned} \tag{6}$$

Substituting back into (5) and eliminating H_x and H_z in the resulting system of equations, one obtains $\partial^2 E_y/\partial z^2 = -k_{z,J}^2 E_y(z)$, for which, taking the origin of z to be in the middle of F, and recalling that for J = S and J = C, $k_{z,J}$ is imaginary, but real for J = F, the solution is

$$\begin{aligned} E_y &= A \exp(ik_{z,F} z) + B \exp(-ik_{z,F} z), \qquad -d/2 \leqslant z \leqslant d/2 \\ E_y &= C \exp[-|k_{z,C}|\,(z - d/2)], \qquad z \geqslant d/2 \\ E_y &= D \exp[|k_{z,S}|\,(z + d/2)], \qquad z \leqslant -d/2 \end{aligned} \tag{7}$$

The boundary conditions are the requirements that E_y and $\partial E_y/\partial z$ are continuous at $z = \pm d/2$, from which the unknowns A, B, C, and D can be eliminated and the eigenvalue equation which must be satisfied by the mode indices N can readily be found:

$$\tan(k_{z,F} d_F) = \frac{(|k_{z,C}| + |k_{z,S}|)\, k_{z,F}}{k_{z,F}^2 - |k_{z,C}| \cdot |k_{z,S}|} \tag{8}$$

[6] TE waves contain the field components E_y, H_x, and H_z (i.e., only the electric field has a transverse component), and TM waves the components H_y, E_x, and E_z.

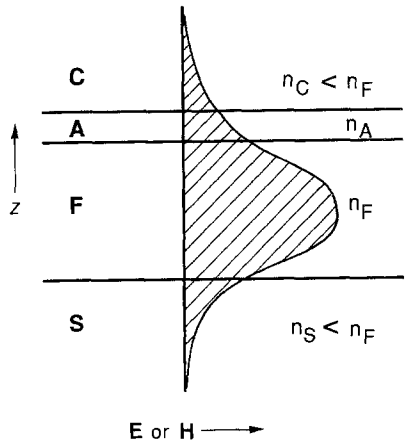

Fig. 2. Electric or magnetic field distribution for a zeroth mode ($m = 0$).

The field distributions in C and S are just exponentially decaying, i.e., evanescent, waves and that in F is sinusoidal (Fig. 2). Corresponding expressions, *mutatis mutandis*, can be found for the TM modes.[13,15]

Now that we have seen how the field distribution in the waveguiding film and its surroundings can be computed, we return to the ray optic treatment in order to obtain more convenient expressions relating the (measurable) mode index N to the optogeometrical parameters (refractive index and thickness) of a thin adlayer A of particles adsorbed at the F, C interface. The starting point is the well-known Fresnel reflection coefficients[7]

$$R_{F,J} = \frac{k_{z,F}/n_F^{2\rho} - k_{z,J}/n_J^{2\rho}}{k_{z,F}/n_F^{2\rho} + k_{z,J}/n_J^{2\rho}} \tag{9}$$

where $k_{z,J}$ is defined analogously to $k_{z,F}$ in (3); since $\sin\theta > n_J/n_F$, $k_{z,J}$ is always imaginary. Using $\Phi_{F,J}$ to denote the phase shift experienced by the wave upon total internal reflection at the F, J interface, we can write

$$R_{F,J} = \exp(i\Phi_{F,J}) \tag{10}$$

and from (9) and (10) we readily find

$$\tan(\Phi_{F,J}/2) = |k_{z,J}|/k_{z,F} \tag{11}$$

for the TE wave. To see that Φ is equivalent to the Goos–Hänchen shift,[16,17] consider light from a slit (whose width $H \gg \lambda$) falling onto the

[7] These results of classical optics can be found in the usual textbooks, e.g., ref. 14.

dielectric discontinuity with angle θ_i. This light may be considered as a superposition of infinitely many infinite elementary plane waves, each of which propagates away from the discontinuity at a slightly different angle θ, the range of θ remaining nevertheless very close to θ_i. The x component of the wave vector of a reflected elementary wave is $k_x = (2\pi/\lambda)\sin\theta$. We now take just two of these waves, the first of which is $\exp[i(k_x x + \Phi)]$, Φ being the phase shift due to reflection. The second wave is reflected with an angle $\theta + \Delta\theta$, and therefore is $\exp\{i[(k_x + \Delta k_x)x + \Phi + \Delta\Phi]\}$. The superposed wave is

$$\begin{aligned}\psi &= \exp[i(k_x x + \Phi)] + \exp\{i[(k_x + \Delta k_x)x + \Phi + \Delta\Phi]\} \\ &= \exp[i(k_x x + \Phi)]\{1 + \exp[i(\Delta k_x x + \Delta\Phi)]\}\end{aligned} \tag{12}$$

and will engender spatial beats with maxima at positions given by $\Delta k_x x + \Delta\Phi = 2\pi\nu$, $\nu = 0, 1, \ldots$. Compare this wave with one reflected geometrically (e.g., at a silver surface), for which Φ is independent of θ_i, i.e., $\Delta\Phi = 0$, and hence the beats appear according to $\Delta k_x x_{\text{geom}} = 2\pi\nu$, $\nu = 0, 1, \ldots$. Subtraction and replacing the differences with differentials yields

$$D = x - x_{\text{geom}} = -d\Phi/dk_x = -(\lambda/2\pi)(d\Phi/d\theta)\cos\theta \tag{13}$$

The complete calculation has been carried out by Artmann[16] and extended by Lotsch.[17]

If a thin adlayer A (composed of a layer of random sequentially absorbed particles) is interposed between the layers F and J, the reflection coefficient $R_{\text{F,J}}$ is modified to become[18]

$$R_{\text{F,A,J}} = \frac{R_{\text{F,A}} + R_{\text{A,J}}\exp(2ik_{z,\text{A}}d_{\text{A}})}{1 + R_{\text{F,A}}R_{\text{A,J}}\exp(2ik_{z,\text{A}}d_{\text{A}})} \tag{14}$$

where $R_{\text{F,A}}$ is given by (9) with J replaced by A (similarly for $R_{\text{A,J}}$) and $k_{z,\text{A}}$ by (3) with F replaced by A. For a second adlayer B, $R_{\text{A,J}}$ in (14) must be replaced by $R_{\text{A,B,J}}$, given by[19]

$$R_{\text{A,B,J}} = \frac{R_{\text{A,B}} + R_{\text{B,J}}\exp(2ik_{z,\text{B}}d_{\text{B}})}{1 + R_{\text{A,B}}R_{\text{B,J}}\exp(2ik_{z,\text{B}}d_{\text{B}})} \tag{15}$$

with obvious (though unwieldy) extensions to any number of additional adlayers.

In order for the ray to propagate for an indefinite distance along the waveguide in the x direction, the condition is that the phase change undergone by the wave on a round trip [i.e., reflection at (F, S), across F to

(F, C), reflection at (F, C), and back again to (F, S)] is equal to zero or an integral multiple of 2π radians. Writing this condition out, we obtain the mode equations for an asymmetric waveguide:

$$2k(n_F^2 - N^2)^{1/2} d_F + \Phi_{F,S} + \Phi_{F,A,C} = 2\pi m \tag{16}$$

with the surroundings denoted explicitly as S and C, and with an adlayer A interposed between F and C. The mode equations (16) give us relations (one per mode) between the effective refractive index N, which can be measured, (see Section 2.2), and the optogeometric parameters of the composite waveguide (comprising support S, waveguiding film F, adlayer A, and cover C).

Substituting the expressions for Φ into (16), and taking advantage of the extreme thinness of A (d_A is of molecular dimensions, i.e., $d_A \ll \lambda$) to linearize the exponentials, after some algebra we obtain the complete mode equations for the four-layer waveguide:[18]

$$\pi m = \frac{2\pi}{\lambda}(n_F^2 - N^2)^{1/2}\left(d_F + d_A \frac{n_A^2 - n_C^2}{n_F^2 - n_C^2}\right)\left[\frac{(N/n_C)^2 + (N/n_A)^2 - 1}{(N/n_C)^2 + (N/n_F)^2 - 1}\right]^{\rho}$$
$$- \arctan\left[\left(\frac{n_F}{n_S}\right)^{2\rho}\left(\frac{N^2 - n_S^2}{n_F^2 - N^2}\right)^{1/2}\right] - \arctan\left[\left(\frac{n_F}{n_C}\right)^{2\rho}\left(\frac{N^2 - n_C^2}{n_F^2 - N^2}\right)^{1/2}\right] \tag{17}$$

For the experimental determination of the mass or number of particles adsorbed comprising adlayer A it is necessary to determine n_A and d_A (see Section 2.4), assuming the adlayer to be isotropic, and hence correctly characterized by a single refractive index n_A. If the remaining parameters in (17) are already known, then it suffices to measure N for just two modes, to allow two equations (17) to be solved simultaneously to yields the two unknown adlayer parameters n_A and d_A.

2.2. Measurement of Effective Refractive Index

Practical applications of integrated optics require some way of coupling beams of light propagating in the external medium into the waveguide (or, conversely, the coupling of a guided wave out of the waveguide into a beam propagating through free space). Coupling may be accomplished using special devices (couplers). One type comprises the direct class, whereby a beam is focused onto an exposed edge of the waveguide, a tricky operation, for the waveguide is very thin (typically a few hundred nm), and the edge is usually rough. The development of devices for coupling beams obliquely incident onto the waveguide was a significant advance. Both prisms and grating have been used as coupling

devices.[15] The basic idea is to match a wave excited at the surface of the device by an incoming beam with that of a possible guided mode. Perturbation of the waveguide effective refractive index (by adlayer formation) in the coupling area will change the optogeometrical parameters (wavelength and angle of incidence onto the device) required for maximum coupling efficiency. For measuring the kinetics of adlayer formation a prism is not practical because it blocks access of particles present in the medium C to the surface of F. For a grating, the coupling efficiency η, defined as (power of guided mode)/(power of incident beam), depends, *inter alia*, on the amplitude h of corrugation, but since the magnitude of η is not critical for the determination of N, h can be small enough to affect negligibly the planarity of the interface if placed at the F,C boundary, and in any case the grating corrugations can equally well be formed at the S,F interface.

As is well known, a grating of periodicity Λ engenders spatial harmonics. If the wave vector component $k' = kn_{\text{air}} \sin \alpha + 2\pi l/\Lambda$ of the diffracted wave ($l = \pm 1, 2, \ldots$ is the diffraction order) engendered by a beam of light falling on the grating with an angle α to the grating normal matches a possible guided mode with wave vector component kN, i.e., $kN = k'$, then that mode will be excited.[20,15,18] Hence we can write down the *incoupling condition* as[18]

$$N = n_{\text{air}} \sin \alpha + l\lambda/\Lambda \tag{18}$$

To determine N, the incoupled power may be measured (e.g., by a photodetector situated at one end of the waveguide) while varying either the angle of incidence onto the grating of the incoming beam or its wavelength.[21] The coupling efficiency can be described by a detuning variable $\bar{N}$,[18]

$$\bar{N} = N - n_{\text{air}} \sin \alpha + l\lambda/\Lambda \tag{19}$$

In the vicinity of $\bar{N} = 0$ it has a resonance of width $\delta\bar{N}$ (Fig. 3), which can be estimated from the optical uncertainty principle $L_x \delta k_x \approx 2\pi$,[18] where L_x is the length of the grating and δk_x the uncertainty of the diffracted wave component in the x direction. Since $\delta k_x = \delta N = \delta\bar{N}$, $\delta\bar{N} \approx \lambda/L_x$. For visible light incident on a grating a few mm long, $\delta\bar{N} \sim 10^{-4}$.

The choice of experimental configuration depends on technical considerations; goniometer technology for the precision measurement of angles is highly developed. When linearly polarized light falls obliquely onto the grating, both TE and TM modes are excited, but at different angles of incidence and can hence be easily separated. The development of precisely tunable diode lasers makes wavelength modulation another option for determining N. The grating may also be used as an output coupler,[22]

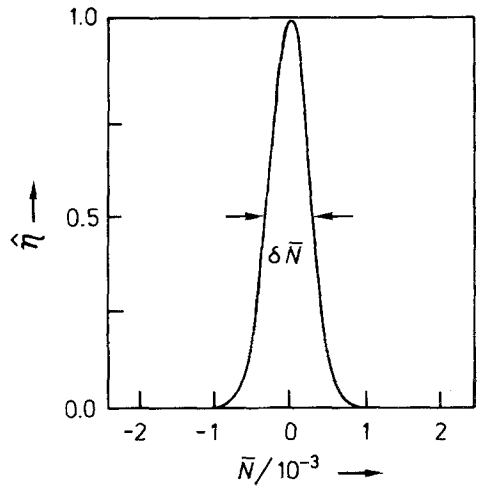

Fig. 3. Normalized coupling efficiency $\hat{\eta}$ as a function of the detuning variable $\bar{N}$ defined by (19).[18]

in which case either wavelength modulation or position-sensitive fixed-wavelength detection can be used.

A different type of configuration for measuring N is the integrated optics interferometer. In the Mach–Zehnder arrangement,[13,21] a single-mode waveguide splits into two separate arms, one of which is subject to, e.g., adsorption engendering a change in N. They then rejoin to form a single waveguide, and the phase shift of the guided mode measured. In the difference interferometer,[23] which does not require microstructuring the waveguide, the time-dependent phase difference between TE and TM modes propagating along a common path is measured.

The sensitivity of the mode index to changes in the optogeometrical parameters of the adlayer can be calculated by (implicit) differentiation of the mode equations (16).[18,24] Some values have been plotted as a function of waveguide thickness d_F by Tiefenthaler and Lukosz.[18] For a typical device, the sensitivity $\partial N/\partial d_A$ increases sharply from zero at the cutoff thickness [the thickness below which, according to (16) or (17), the mode cannot exist[13]] reaches a maximum, and then slowly decays. Successive modes $m = 0, 1, 2,...$ have successively lower maxima (see Fig. 4). Optimal sensitivity for two modes. sufficient for determining the number of adsorbed particles, is attained by using a thin ($d_F \approx 200$ nm) monomode waveguide with which TE_0 and TM_0 can be measured.

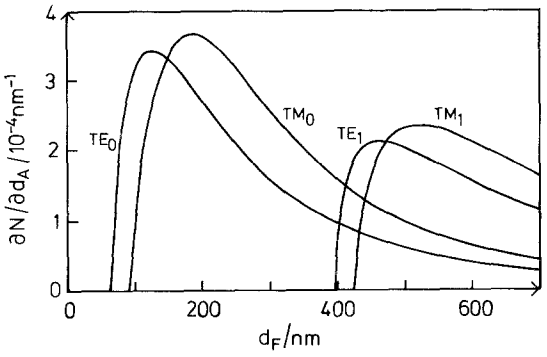

Fig. 4. Sensitivities for changes in adlayer thickness for various modes.[18] Computed for an adlayer formed by particles with $n_A = 1.5$ deposited on a waveguide with $n_F = 1.75$ (supported on glass with $n_S = 1.47$) from an aqueous solution ($n_C = 1.333$); $\lambda = 632.8$ nm.

2.3. Calculation of Mass from the Optical Data

The surface coverage (mass or number of particles per unit area) M is defined as

$$M = \int_0^\infty [c_s(z) - c_{\text{bulk}}]\, dz \tag{20}$$

where c_s is the surface (adsorbed) concentration of the species of interest, and c_{bulk} its bulk concentration ($c_s \to c_{\text{bulk}}$ as $z \to \infty$). We assume that the adlayer A possesses only weak fluctuations and is amenable to a mean-field treatment. Although this assumption may not apply to an adlayer of polymers composed of long chains of jointed segments, it is reasonable in the present case of interest, i.e., a collection of randomly adsorbed, compact particles (e.g., globular proteins), forming at most a monolayer. The adlayer may then be described by a mean concentration c_A and mean thickness d_A (Fig. 5). The adlayer is assumed to be laterally uniform, but this requirement is not very stringent; the distribution of particles should be symmetrical with respect to translation over distances of order λ. For the uniform adlayer, (20) can be simplified to

$$M = (c_A - c_{\text{bulk}})d_A \tag{21}$$

Frequently $c_A \gg c_{\text{bulk}}$, and one can write

$$M = c_A d_A \tag{22}$$

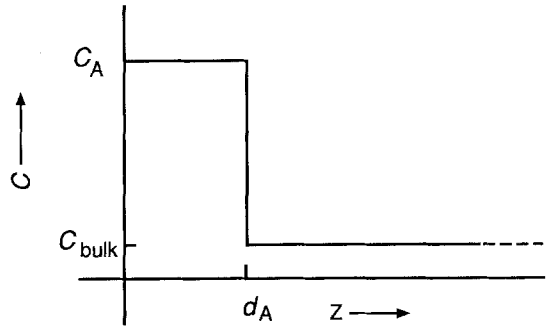

Fig. 5. Idealized adlayer (see text).

The refractive index of the layer n_A is related to c_A according to[25]

$$n_A = n_C + c_A \frac{dn}{dc} \tag{23}$$

where n_C is the refractive index of the medium in which the particles to be adsorbed are suspended. This equation is assumed to be valid both in the bulk and in the thin adlayer. The coefficient dn/dc depends on the polarizability of the particles, and hence on their chemical constitution; it mayh readily be determined to high precision using a bulk solution of the particles in a Rayleigh interferometer.[26]

Eliminating c_A between (22) and (23), one obtains

$$M = d_A \frac{n_A - n_C}{dn/dc} \tag{24}$$

which is used to calculate M from the experimentally determined d_A and n_A.[25,27]

3. WAVEGUIDE MATERIALS AND FABRICATION

Materials. Dielectric metal oxides (TiO_2, Ta_2O_5, etc.) are suitable for manufacturing high-refractive-index waveguides for RSA applications. Since it is usually desirable to carry out experiments with adsorbing particles suspended in aqueous solutions (Section 5) nonoxide materials (e.g., Si_3N_4, GaAs) are unsuitable because they may be extensively oxidized, hydrolyzed, or corroded in water. The oxides are also convenient because their surface properties, especially charge density, can be readily modified by changing solution conditions (pH, ionic strength). As shown in

Section 2.3, monomode waveguides are advantageous if only two unknowns (thickness and refractive index of the adsorbed adlayer, from which the mass or number of particles can be calculated) need to be determined simultaneously, because the sensitivity ($\partial N/\partial w$, where w is one of the two unknowns) is higher than for multimode waveguides (Fig. 4). Because of the thinness of monomode waveguides (typically 100–200 nm), the waveguiding layer F must rest on a support S, typically glass 500 μm thick. The layer F can be fabricated using techniques such as chemical vapor deposition, pyrolysis of sol–gel coatings, and sputtering.[21] Polymers can be deposited using spin coating; but thick layers (~ 1 μm), exceeding the penetration depth [Eq. (4)] of the evanescent field, are produced, and hence the mode indices are no longer sensitive to the presence of an adsorbed adlayer. A further possibility is to use the Langmuir–Blodgett technique[28] to build up suitably thick waveguiding layers.[29]

Grating fabrication. The ideal grating for the application described in this article is a compromise between corrugations of amplitude small enough to perturb negligibly the planarity of the surface (if the grating is at the F,J interface) and propagation of the guided modes, and large enough to couple enough light into the waveguide from the incoming beam to be detected at the end of the waveguide (or conversely, couple enough light out of the waveguide, if the outcoupling configuration is being used).

The technological advance of low-cost grating couplers has greatly facilitated the experimental situation, which, because of contamination problems, etc., often requires that fresh gratings are used for each measurement. Waveguides fabricated inexpensively from pyrolyzing dip-coated sol–gel films have been found to be adequate for RSA experiments. The grating coupler may be conveniently embossed into the F,C interface before hardening the waveguiding film.[30,31]

Surface characterization. The physical and chemical nature of the waveguide surface characterizes to a great extent the kinetics of adsorption of particles, independently of the random sequential nature of the process. The rugosity determines the mass transport to the surface (Section 4.1)—the ideal is a smooth, planar surface—and the surface chemistry affects the probability of particles sticking upon collision, their lateral mobility, and postadsorption conformational relaxation. These factors are important in extensions to the basic RSA model and in natural RSA processes.

Although metal oxides show long-term stability when immersed in water, the oxide and hydroxyl groups at the surface may be ionized (protonated or deprotonated) or suffer ionic exchange when the waveguide is first placed in contact with an aqueous solution. The surface charge

density therefore depends upon the pH and ionic strength of the solution, as well, of course, as on temperature.[32] The behavior of the oxides of titanium and silicon has been extensively documented.[33,34]

Surface modification. The moderate reactivity of metal oxide surfaces is very useful for modulating parameters important in RSA models, such as the surface mobility, adhesion, and conformational relaxation of the adsorbed particles, which may interact with the surface via many different varieties of (electromagnetic) forces—dispersion (van der Waals), electrostatic (double layer, ion-pair, dipole–dipole interactions), or by electron exchange (chemical bond formation). Multivalent metal ions are useful for modifying the surface charge of the waveguide and may be incorporated into the waveguide surface by bringing it into contact with a solution of an appropriate metal salt.[35] Alkyl groups can be covalently attached to the surface, often by simply exposing it to the vapor of simple alkyl silane derivatives, and are useful for increasing the affinity of the surface for hydrophobic particles; the same technique can be used to incorporate other chemical functionalities in the surface. An important and general way of controlling the surface is via the Langmuir–Blodgett (LB) technique,[28] which is especially especially useful for fine tuning the chemical properties[36] or reflection phase shifts[29] of a planar waveguide, because a single or few monolayers, for which the quality of the deposition is high, suffice to obtain the desired effect. Such films may also eliminate small rugosities on the surface.

Surface heterogeneity. Most applications of integrated optics do not require great uniformity of material properties at the atomic scale. Scattering due to defects is a nuisance for transmission applications, but in the present case is unimportant, because the guided wave only has to travel a distance ~ 1 cm before detection. Nevertheless, adsorption kinetics may greatly depend on the chemical properties of the surface at the atomic scale. It is often assumed that particle-surface bond energies are everywhere identical; a distribution of adsorption energies leads to adsorption kinetics different from the case of a surface where the energy is everywhere identical.[37,38]

4. MASS TRANSPORT WITHIN ADSORPTION CELLS

In theory, or numerical simulations, the kinetics of the RSA process are scaled with the number of attempts to deposit a particle. In an actual experiment, a solution containing the particles is placed in or driven through a cuvette, one wall of which is formed by the grating region of the waveguide (Fig. 6). The frequency of attempts thus depends to a very great

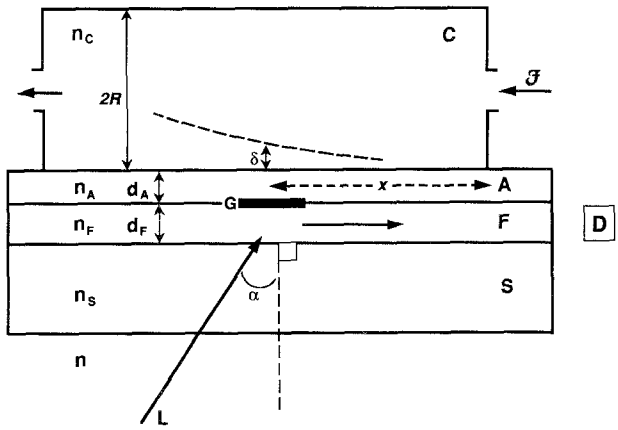

Fig. 6. Schematic diagram of a cuvette into which liquids containing particles may be introduced. The optical waveguide, set up for measurement of the incoupling angle, forms one wall of the cuvette. L, linearly polarized incoming light beam; G, diffraction grating; D, photodetector. For other symbols, see text. Typically, the grating might be 2 mm long, the incoming beam less than 1 mm in diameter, $R \approx 1$ mm, and the flow rate $\mathcal{F} \approx 0.1$ mm^3/sec.[41]

degree on purely hydrodynamic factors, and the experimental arrangement should be such as to facilitate the analysis of these factors. This can be fulfilled far more easily with a planar substrate than with a collection of comminuted substrate particles as in the packed bed technique,[39,40] in which only an average flux to the surface can be estimated.

When the solution (or suspension) is in a state of equilibrium, the temperature T, pressure p, and chemical potentials μ of the constituents are constant and there is no macroscopic motion (flow). Any departure from equilibrium will be assumed to be caused by differences in solute concentration c between two points in the liquid, or its macroscopic motion, or both. The transport of the solute particles is governed by two distinct mechanisms: molecular diffusion as a result of concentration differences, and the entrainment of particles in the flow of the liquid. The combination of the two is called convective diffusion.[42]

4.1. Closed Cells

In this case transport of particles in the liquid is governed purely by molecular diffusion. Initially the particle concentration is everywhere uniform, but since any particle arriving at the surface sticks irreversibly, the concentration (of the particles in solution) at $t > 0$ will be zero at the

surface. For a semi-infinite cylinder, bounded at one end by the adsorbing surface, the flux is[43]

$$I = 2c_{\text{bulk}}(Dt/\pi)^{\alpha} \tag{25}$$

with $\alpha = 0.5$, and where D is the diffusion coefficient of the particles, defined by

$$D = \left(\frac{\partial \mu}{\partial c}\right)_{T,p} \tag{26}$$

This equation may be used even for a macroscopically small finite cylinder (with a reflecting barrier at the other end), provided it is still large with respect to molecular dimensions, and that there is no significant depletion of the solution during adsorption.[44] Otherwise, more complicated and less convenient equations must be used.[44] If the sticking probability of a particle which arrives at the surface is less than unity, (25) must be modified.[36] For rugose surfaces with self-similar corrugations characterized by a fractal dimension d, the exponent α in (25) becomes $(d-1)/d$.[45,46]

4.2. Open (Flow) Cells

When the available volume of solution permits, it is better to arrange to have it flowing through the cuvette, for the frequency of adsorption attempts is then uniform in time (i.e., sidereal time). Another advantage of flow cells is that particles failing to adsorb on their first attempt will tend to be swept away, whereas if transport is purely diffusive, a particle which arrives at the surface and fails to adsorb at its first attempt will probably make several fresh attempts in the vicinity of the first before diffusing away.[47,48] Basic RSA assumes the absence of such correlations between attempts.[3]

The macroscopic motion of the liquid is determined by the volume and surface forces acting on it, and can be described by the appropriate equations of motion and continuity.[42] As noted above, mass transport (represented by the flux $\mathbf{I}$ to or across a plane of unit area) is governed by both convection and molecular diffusion, corresponding, respectively, to the first and second terms on the right hand side of

$$\mathbf{I} = c\mathbf{v} - D\nabla c \tag{27}$$

where $\mathbf{v}$ is the vector describing the volume of liquid passing through the plane in unit time. Concentration and chemical potential gradients are assumed to be small.

The macroscopic flow is characterized by the dimensionless Reynolds number Re, defined by

$$\mathrm{Re} = Ux/\nu \tag{28}$$

where U is a characteristic velocity (e.g., of the fluid flowing through the cell) and x a characteristic length. Flow is laminar when $\mathrm{Re} < \sim 2500$, and otherwise turbulent.[42] For typical experimental arrangements (Fig. 6), $\mathrm{Re} \sim 1$.

When a liquid flow past a solid surface, the liquid experiences viscous drag and its velocity drops to zero at the surface.[8] One may divide the liquid into two regions, a narrow boundary region where the velocity changes rapidly, of thickness[42]

$$\delta_0 \approx 1.7(\nu x/U)^{1/2} \tag{29}$$

where x is the distance from the leading edge of the surface, and the region far from the surface where the velocity is constant.

The relationship between convective and diffusive transport is described by another dimensionless ratio, the Peclet number Pe:

$$\mathrm{Pe} = Ux/D \tag{30}$$

The small diffusion coefficients of particles of molecular size in liquids results in their being characterized by large Peclet numbers even at slow rates of fluid flow. In such a regime, the liquid can again be divided into two regions: a region of rapidly changing concentration near the adsorbing surface, the diffusion boundary layer, of thickness[42]

$$\delta \approx 3(D/\nu)^{1/3}(\nu x/U)^{1/2} \tag{31}$$

where x is the distance along the surface from its leading edge; and a region of constant particle concentration distant from the surface. The ratio δ_0/δ is therefore equal to $(\nu/D)^{1/3}$, i.e., $\mathrm{Pr}^{1/3}$, where the Prandtl number Pr is given by the ratio Pe/Re, i.e., independent of the flow velocity or characteristic dimensions. A high value of Pr means that convection predominates over diffusion even at low flow rates. For $\mathrm{Pr} \approx 1000$, a typical value for small molecules in water, the hydrodynamic boundary layer is about ten times thicker then the diffusion boundary layer (Fig. 7). Under these conditions convective transport predominates over diffusive. Close to the surface, however, the final stage of transport through the fluid whose velocity is close to zero is diffusive, and approximately equal to

$$I = Dc_{\mathrm{bulk}}/\delta \tag{32}$$

[8] For recent numerical simulations bearing on this assumption, see ref. 49.

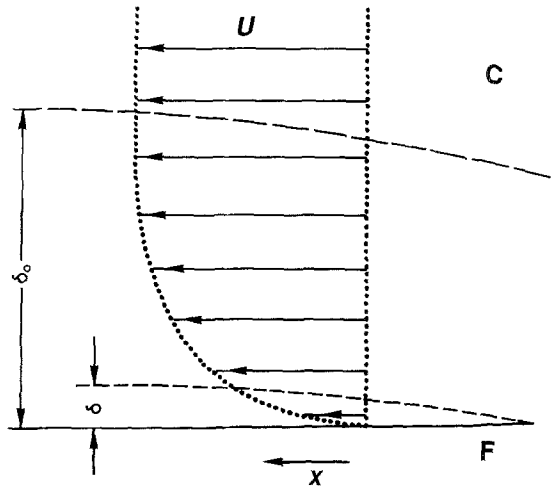

Fig. 7. Diagram of the fluid velocity profile in the vicinity of the waveguide F. δ is the thickness of the diffusion boundary layer, and δ_0 the thickness of the hydrodynamic boundary layer.

i.e., of the same form as in Nernst's theory, except that the thickness of the diffusion boundary layer depends on the velocity and (kinematic) viscosity of the liquid and the distance from the leading edge of the surface.[45,50]

Where the dimensions of the cuvette are small enough for the adsorbing surface (the waveguide) to be considered one wall of a tube (whose cross section we will suppose approximates to a circle with radius R), then, as first shown by Poiseuille, the fluid will adopt a parabolic velocity profile $U(z) = U_{max}(1 - z^2/R^2)$ due to viscous drag at the walls. This profile is not, however, established immediately; when the fluid first enters the tube the velocity profile is flat. The tube may be divided into three sections along the direction of the flow: the hydrodynamic inlet section, of length $h \sim 0.1R \cdot \mathrm{Re}$, in which (31) and (32) can be used to compute the transport of solute, the diffusion inlet region, of length $H \sim R \cdot \mathrm{Re} \cdot \mathrm{Pr}$, in which solute transport is again given by (32), but with the thickness of the diffusion boundary layer given by:[42],[9]

$$\delta = (3/2)(DxR/U_{max})^{1/3} \tag{33}$$

and hence the flux per unit area by

$$I = (2/3)c_{bulk} D^{2/3}[U_{max}/(xR)]^{1/3} \tag{34}$$

[9] These expressions are valid for $\nu \gg D$, i.e., when the diffusion boundary layer is much thinner than the hydrodynamic boundary layer.

and finally the region in which the Poiseuille profile is properly developed. Since $Pr \gg 1$, not only is $H \gg h$, but in most cases encountered, H will usually be much longer then the entire length of the tube, i.e., the Poiseuille profile is never properly established, and this region need not be considered here.

5. RECENT AND EXPECTED RESULTS

Proteins as adsorbing particles. Proteins are very attractive molecules for use in RSA experiments. Typically they are spheroidal with diameters of a few tens of nanometers, but highly elongated and branched forms several hundred nm long are also known.[44] Unlike colloidal particles, which always show some size dispersity, a protein is a molecule of a definite chemical structure whose congeners are identical. Modern methods of purification and handling mean that homogeneous populations of identical molecules can readily be obtained. For the 200 or so proteins whose crystal structures have been worked out, surface chemistry and topology are precisely known. From the shape and mass data important hydrodynamic parameters such as the diffusion coefficient can be calculated. Native proteins offer an astonishing variety of chemical species, often with subtly different surface properties, and modern techniques of molecular biology can be used to make small changes ("mutations"), even of a single atom out of the 10,000 or so in an average protein, at a precisely known location, and an arbitrarily large collection of identical congeners of the modified protein can be prepared. The adsorption behavior of proteins appears to display a richness commensurate with their manifold functions in living organisms.[10] Not only do their sticking probabilities to adsorbing surfaces and to each other depend upon their surface chemistries and solutions, but, again in contrast to latex and other colloidal particles, proteins possess a complex internal structure and may change their shape other attributes, including sticking probability, following adsorption.[51,52]

In a recently reported example,[41] adsorption of the almost spheroidal protein transferrin to $SiTiO_2$ planar waveguides was shown to be well described, at any given concentration, by the Schaaf–Talbot expression for

[10] Protein adsorption at solid surfaces has attracted intense interest from investigators interested in physiological and medical implications. Nevertheless, despite a great volume of work,[51] very little is actually usable in connection with testing RSA theories. The main drawbacks are: that the actual amounts of material adsorbed were either not known in terms of absolute mass or numbers of particles, or known with too high uncertainty to permit more than qualititative inferences; that the systems investigated were too complex, consisting of ill-defined natural products or mixtures; or that kinetic data were too sparse.

RSA of disks.[53,54] A protein such as transferrin is extremely soluble in water and shows no tendency to aggregate in solution. It therefore meets the basic RSA condition, that any particle arriving near an area of the surface where no gap large enough for adsorption is available will diffuse back into the bulk solution. Nevertheless, the area per molecule was found to depend on protein concentration, implying that even in this simple case two different orientations or conformations of adsorbed molecules were possible and that relaxation from one to the other occurred. This work is now being extended to other proteins.[55]

Proteins are too small for their transport to the adsorbing surface to be affected by terrestrial gravitational fields, at least on the time scales of reasonable experiments, but are usually ionized, depending on amino acid composition and solution pH. When the metal oxide surface of waveguides are exposed to aqueous solutions, hydroxyl groups are ionized, leaving a negatively charged surface, neutralized by a space charge of positive ions in the adjacent solution (electrical double layer).[34] At moderate salt concentrations the surface charge is neutralized within a distance of one or two solvent molecule diameters from the surface, i.e., a distance much smaller than the protein diameter, but at low salt concentrations the electrostatic force between the surface and the protein must be included in (27). Since the charge on a protein is rarely homogeneously distributed (there may be patches of positive and negative charges on the same molecule), a charge

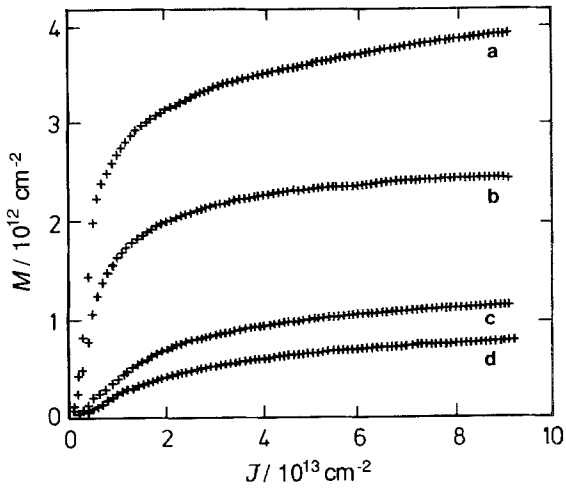

Fig. 8. Experimental results showing the kinetics of adsorption of apotransferrin from pure water (a) and buffered solutions (pH 8.0) of different ionic strengths; (b) 2 mM tris-HCl; (c) 10 mM tris-HCl; (d) 10 mM tris-HCl + 0.1 M NaCl.[60]

on the adsorbing surface may orient arriving molecules. Multiple weak chemical bonds (hydrogen bonds)[56] are important for binding proteins to hydrated oxide surfaces. Particularly in aqueous solutions, solvent-mediated interactions may occur (the hydrophobic effect).[57–59] Both hydrogen bonds and the hydrophobic effect may be important in determining the relaxation processes which follow the initial arrival and adsorption of the protein at a surface, and these interactions may be modulated by varying the ionic strength of the bulk solution (Fig. 8).[60]

Recently, very large and elaborate proteins, important in the formation of basement membranes in multicellular organisms, have been purified and characterized.[61] They are expected to show complex adsorption behavior, not yet investigated theoretically. It seems to be typical that a small change in solution conditions engenders a significant change in adsorption behavior. For example, in the absence of calcium ions, the tetrabrachiate extracellular matrix protein laminin forms monolayers at the solid–solution interface, but multilayers in the presence of calcium.[62]

6. CONCLUSIONS

Light may be confined in a thin dielectric medium bounded by media with lower refractive indices (the basis of integrated optics). The light propagates in the thin film by total internal reflection at the refractive index discontinuities bordering the film. The electric field distribution in the film is a standing wave whose eigenvalues N depend on the bulk waveguide parameters (fixed) and the boundary conditions (variable), i.e., the polarizability profile at the solid–solution interface. N can be conveniently determined by measuring the angle of incidence of an external beam onto a grating coupler incorporated into a waveguide designed for optimal incoupling [Eq. (18)]. The dependence of the eigenvalues on the boundary conditions is described by the mode equations (17). If an adlayer A is interposed between the film and the covering medium, its parameters (thickness and refractive index) also enter into the mode equation, and, provided the other waveguide parameters are known, can be determined from the measurement of N for two modes. If the polarizability of the particles constituting the adlayer is known, the surface density of adsorbed adlayer particles can be calculated [Eq. (24)]. Adsorption is initiated by placing a cuvette into which a suspension of the adsorbable particles can be introduced over the grating region, which thus forms one wall of the cuvette.

Assumptions made in the derivation of the working equations [Eqs. (17), (18), and (24)]. All the layers in the multilayer waveguide are assumed to be isotropic, linear, nonmagnetic, nonconducting, and charge-

free. This is only an approximation. Many biological structures are birefringent[63]; however, most commonly the birefringence is due to arrays of oriented elongated particles (proteins) which are intrinsically optically isotropic. Since up until now RSA has mainly been concerned with randomly arranged spheres, birefringence of the adlayer is not expected. Nevertheless, as more elaborate adsorbing objects are investigated, the birefringence of the adlayer will have to be taken into account. This will require the measurement of the effective refractive indices of three modes, and the isotropic n_A in Eq. (17) will have to be replaced by $n_{A,\rho}$, $\rho = 0$ corresponding to the TE modes (ordinary ray) and $\rho = 1$ related to the TM modes (extraordinary ray).

The assumptions of a charge-free and nonconducting adlayer will often be violated because most experiments are carried out with proteins dissolved in solutions of aqueous electrolytes, and both the proteins and the surface of the waveguide will be ionized.[32] The charge and conductivity can be taken care of by replacing the real refractive indices characterizing the layers by complex ones; typically only a very small imaginary part will be required. The mode equations can then be derived in exactly the same way from the Fresnel reflection coefficients, but now they will be more complicated, and must be solved numerically. Sample calculations show that the error introduced by the assumption of neither charge nor conductivity is much less than the current precision of the effective index measurements. The reason is, of course, that most of the energy of the guided waves flows through the layer F, for which the assumptions hold. A similar argument applies to adlayers which adsorb some of the guided radiation.

Equation (17) is the linearized form of the full mode equation, valid for adlayer thicknesses up to 50–100 nm, depending upon the degree of precision required, i.e., adequate for protein monolayers and oligolayers of proteins which typically have diameters ~ 10 nm. For thicker layers, the full, nonlinear form has to be used,[18] and solved numerically.

The use of Eq. (24) assumes that the adlayer has a uniform refractive index profile perpendicular to the interface. For a monolayer of spherical particles, this is correct. If several orientations of the particles are possible, the layer can be decomposed into two or more layers,[64] and the appropriate additional number of modes measured to characterize them. Arbitrary profiles can also be dealt with.[65]

Equation (24) further assumes that n_A is a linear function of c_A. The linearity has been tested in bulk protein solutions up to a concentration of 0.4 g/cm^3, with no indication of any deviation from linearity.[25] For a protein forming a layer 10 nm thick, this corresponds to $M = 0.4\ \mu$g/cm^2. For a typical protein of molecular mass 60,000 g/mole, this corresponds to

4×10^{12} molecules/cm^2, which represents the upper limit of adsorption in typical experiments (see Fig. 8).

Long-range order is absent in the structures produced by RSA, and there is no experimental evidence that proteins form regular arrays which could interfere with the propagation of guided modes in the waveguide. On the contrary, since the characteristic dimensions of proteins are much smaller than λ, the surface film constitutes, at least to a first approximation, an effective medium well describable by a thickness and refractive index.

The working equations written down in the forms given above have the advantage that they can be solved analytically to determine M from the experimentally measured quantities. If the assumptions used in deriving them are relaxed, the equations become more complicated, and must be solved numerically, but the basic principle of the measurement is unchanged. Apart from their experimental simplicity, one of the main advantages of the integrated optics methods discussed in this review over other techniques which have been used in the past to measure the mass of adsorbed material at surfaces is the robustness of the derivations of the working equations under conditions likely to be encountered in practice.[66]

ACKNOWLEDGMENTS

I am indebted to R.-I. Stohn for having calculated some field distributions in multilayer waveguides with complex refractive indices, and to Prof. A. E. Shapiro for correspondence on Newton's work on optics; it is a pleasure to thank M. Jäggi for having drawn the figures.

REFERENCES

1. A. Rényi, *A Magyar Tudományos Akadémia Matematikai Kutató Intézetének Közleményei* **3**:109 (1958).
2. M. C. Bartelt and V. Privman, *Int. J. Mod. Phys.* **5**:2883 (1991).
3. B. Senger, J.-C. Voegel, P. Schaaf, A. Johner, A. Schmitt, and J. Talbot, *Phys. Rev. A* **44**:6926 (1991).
4. J. Bafaluy, B. Senger, J.-C. Voegel, and P. Schaaf, *Phys. Rev. Lett.* **70**:623 (1993).
5. M. von Smoluchowski, *Phys. Z.* **17**:557 (1916).
6. G. Y. Onoda and E. G. Liniger, *Phys. Rev. A* **33**:715 (1986).
7. M. H. Kao, A. G. Yodh, and D. J. Pine, *Phys. Rev. Lett.* **70**:242 (1993).
8. J. Lohne, *Centaurus* **6**:113 (1959).
9. I. Newton, *Philosophiae naturalis principia mathematica*, Lib. 1, Sect. XIV, Prop. XCVI, Theor. L (Royal Society, London, 1687).
10. I. Newton, *Opticks*, 4th ed., Book 3, Qu. 29 (William Innys, London, 1730).
11. F. Goos and H. Hänchen, *Ann. Phys. (6)* (N.Y.) **1**:333 (1947).
12. M. J. Adams, *An Introduction to Optical Waveguides* (Wiley, Chichester, England, 1981).

13. A. Ghatak and K. Thyagarajan, *Optical Electronics* (Cambridge University Press, 1989).
14. F. A. Jenkins and H. E. White, *Fundamentals of Optics*, 2nd ed. (McGraw-Hill, New York, 1950).
15. P. K. Tien, *Rev. Mod. Phys.* **49**:361 (1977).
16. K. Artmann, *Ann. Phys.* **2**:87 (1948).
17. H. K. V. Lotsch, *J. Opt. Soc. Am.* **58**:551 (1968).
18. K. Tiefenthaler and W. Lukosz, *J. Opt. Soc. Am. B* **6**:209 (1989).
19. A. A. Spikhalskii, *Opt. Quantum Electronics* **18**:103 (1986).
20. Lord Rayleigh, *Proc. R. Soc. Lond. A* **79**:399 (1907).
21. O. Parriaux, Guided wave electromagnetism and opto-chemical sensors, in *Fiber Optic Chemical Sensors and Biosensors*, Vol. I, O. S. Wolfbeis, ed. (CRC Press, Boca Raton, Florida, 1991).
22. W. Lukosz and Ch. Stamm, *Sensors Actuators A* **25–27**:185 (1991).
23. W. Lukosz, Ph. M. Nellen, Ch. Stamm, and P. Weiss, *Sensors Actuators B* **1**:585 (1990).
24. J. J. Ramsden, *Sensors Actuators B* **15–16**:439 (1993).
25. J. A. de Feijter, J. Benjamins, and F. A. Veer, *Biopolymers* **17**:1759 (1978).
26. W. Nebe, *Analytische Interferometrie* (Geest & Portig, Leipzig, 1970).
27. W. Lukosz and K. Tiefenthaler, *Sensors Actuators* **15**:273 (1988).
28. K. B. Blodgett and I. Langmuir, *Phys. Rev.* **51**:964 (1937).
29. C. W. Pitt and L. M. Walpita, *Thin Solid Films* **68**:101 (1980).
30. P. P. Herrmann and D. Wildmann, *IEEE J. Quantum Electronics* **QE-19**:1735 (1983).
31. W. Lukosz and K. Tiefenthaler, *Opt. Lett.* **8**:537 (1983).
32. T. W. Healy and L. R. White, *Adv. Colloid Interface Sci.* **9**:303 (1978).
33. D. E. Yates and T. W. Healy, *Trans. Faraday Soc.* **76**:9 (1980).
34. R. J. Hunter, *Zeta Potential in Colloid Science* (Academic Press, London, 1981).
35. J. J. Ramsden, D. U. Roemer, and J. E. Prenosil, in *Proceedings 6th European Conference on Integrated Optics, Neuchâtel* (1993).
36. J. J. Ramsden and P. Schneider, *Biochemistry* **32**:523 (1993).
37. S. Z. Roginskii, *Adsorptsiya i Kataliz na Neodnorodnykh Poverkhnostakh* (Izd. AN SSSR, Moscow, 1948).
38. E. A. Kulik, I. D. Kalinin, and B. I. Sevastyanov, *Zh. Fiz. Khim.* **65**:2230 (1991).
39. J. D. Aptel, J. C. Vogel, and A. Schmitt, *Colloids Surfaces* **29**:359 (1988).
40. G. Leaver, J. A. Howell, and J. R. Conder, *J. Chromatography* **590**:101 (1992).
41. J. J. Ramsden, *Phys. Rev. Lett.* **71**:295 (1993).
42. V. I. Levich, *Physicochemical Hydrodynamics* (Prentice-Hall, Englewood Cliffs, New Jersey, 1962).
43. J. Crank, *The Mathematics of Diffusion*, 2nd ed. (Clarendon Press, Oxford, 1975).
44. J. J. Ramsden, *J. Phys. Chem.* **96**:3388 (1992).
45. P.-G. de Gennes, *C. R. Acad. Sci. Paris (II)* **295**:1061 (1982).
46. T. Pajkossy, *Phys. Rev. B* **42**:709 (1990).
47. E. Rabinowitch and W. C. Wood, *Trans. Faraday Soc.* **32**:1381 (1936).
48. E. Rabinowitch, *Trans. Faraday Soc.* **33**:1225 (1937).
49. M. Sun and C. Ebner, *Phys. Rev. Lett.* **69**:3491 (1992).
50. V. I. Levich, *Disc. Faraday Soc.* **1**:37 (1947).
51. J. D. Andrade and V. Hlady, *Adv. Polymer Sci.* **79**:1 (1986).
52. E. A. Kulik, I. D. Kalinin, and B. I. Sevastyanov, *Zh. Fiz. Khim.* **65**:2234 (1991).
53. P. Schaaf and J. Talbot, *Phys. Rev. Lett.* **62**:175 (1989).
54. P. Schaaf and J. Talbot, *J. Chem. Phys.* **91**:4401 (1989).
55. R. Kurrat, J. J. Ramsden, and J. E. Prenosil, *Trans. Faraday Soc.*, to appear.
56. L. C. Allen, *Proc. Natl Acad. Sci. USA* **72**:4701 (1975).

57. A. B. Meggy, *J. Soc. Dyers Colorists* **66**:510 (1950).
58. N. Muller, *Acc. Chem. Res.* **23**:23 (1990).
59. C. J. van Oss, in *Protein Interactions*, H. Visser, ed. (VCH, Weinheim, 1992).
60. J. J. Ramsden and J. E. Prenosil, *J. Phys. Chem.*, to appear.
61. J. Engel, *Biochemistry* **31**:10643 (1992).
62. J. J. Ramsden, *Biopolymers* **33**:475 (1993).
63. G. Oster, in *Physical Techniques in Biological Research*, G. Oster and A. W. Pollister, eds. (Academic Press, New York, 1955), Vol. 1, Chapter 8.
64. P. Schaaf and Ph. Dejardin, *Colloids Surfaces* **31**:89 (1988).
65. J. C. Charmet and P. G. de Gennes, *J. Opt. Soc. Am.* **73**:1777 (1983).
66. J. J. Ramsden, *Q. Rev. Biophys.*, to appear.